Molecular Therapy
Nucleic Acids
Original Article

Age-associated changes in microglia and astrocytes ameliorate blood-brain barrier dysfunction

Jie Pan,[1,2] Nana Ma,[1] Jie Zhong,[3] Bo Yu,[4,5] Jun Wan, Ph. D,[1,6] and Wei Zhang[1]

[1]Greater Bay Biomedical Innocenter, Shenzhen Bay Laboratory, Shenzhen, Guangdong Province, China; [2]Department of Pathology and Neuropathology, Stanford University School of Medicine, CA 94305, USA; [3]Shenzhen Key Laboratory for Neuronal Structural Biology, Biomedical Research Institute, Shenzhen Peking University - The Hong Kong University of Science and Technology Medical Center, Shenzhen, Guangdong Province, China; [4]Shenzhen Key Laboratory for Translational Medicine of Dermatology, Biomedical Research Institute, Shenzhen Peking University - The Hong Kong University of Science and Technology Medical Center, Shenzhen, Guangdong Province, China; [5]Department of Dermatology, Peking University Shenzhen Hospital, Shenzhen, Guangdong Province, China; [6]Department of Biology, School of Life Sciences, Southern University of Science and Technology, Shenzhen, Guangdong Province, PRC

Blood-brain barrier (BBB) dysfunction is associated with an accumulation of neurotoxic molecules and increased infiltration of peripheral cells within the brain parenchyma. Accruing evidence suggests that microglia and astrocytes play a crucial role in the recovery of BBB integrity and the corralling of infiltrating cells into clusters after brain damage, but the mechanisms involved remain unclear. Intriguingly, the results of flow cytometry and immunofluorescence analyses have shown that BBB permeability to peripheral cells is substantially enhanced during normal aging at 12 months in mice. Thus, we used the SMART-seq2 method to perform RNA sequencing of microglia and astrocytes at five time points before and immediately after the BBB permeability change. Our comprehensive analyses revealed that microglia are characterized by marked alterations in the negative regulation of protein phosphorylation and phagocytic vesicles, whereas astrocytes show elevated enzyme or peptidase-inhibitor activity in the recovery of BBB function. Moreover, we identified a cassette of key genes that might ameliorate the insults of pathophysiological events in aging and neurodegenerative disease.

INTRODUCTION

Aging and neurological/psychiatric disorders are known to be associated with defective blood-brain barrier (BBB) function.[1,2,1] BBB breakdown facilitates entry into the brain of neurotoxic blood-derived products and pathogens and has been linked to inflammatory and immune responses that can induce neuronal injury, synaptic dysfunction, and loss of neuronal connectivity. BBB disruption also facilitates leukocyte infiltration, which leads to glial cell death, axonal damage, lesion development, and therefore cerebrovascular dysfunction results in memory impairment, acceleration of neurovascular damage, and exacerbation of the progression of neuropathology in the central nervous system (CNS). Thus, critical demand exists for new therapies that minimize peripheral immune factors and limit the infiltration of peripheral immune cells into the brain.

The neurovascular unit, which comprises brain endothelial cells, pericytes, astrocytes, and microglia, primarily confers the low paracellular permeability of the BBB.[1,3,4] The tight cell-to-cell contacts that these cell types establish with each other restrict the entry of red blood cells, leukocytes, and plasma components into the brain parenchyma and ensure the export of potentially neurotoxic molecules from the brain to the blood.[5,6] The site of the anatomical BBB is composed of a continuous monolayer of endothelial cells that are connected by tight junctions (TJs) and adherens junctions (containing proteins such as claudin, occludin, and zonula occludens [ZO] 1, ZO2, ZO3, and other isoforms).[7,8] The interactions among the endothelial cells, pericytes, and glial cells are crucial for the formation and maintenance of the highly regulated CNS internal milieu.[5,9,10]

Astrocytes play a dual role in limiting the entry of peripheral substances into the CNS: permeability factors secreted by reactive astrocytes open the BBB by disrupting endothelial TJs,[11,12] but reactive astrocytes also perform a protective function by upregulating classical TJ proteins and junctional adhesion molecule A at the glia limitans (GL) and using TJ proteins to corral activated T lymphocytes into distinct clusters.[13,14] However, the upregulated TJ proteins are cleaved by proteases secreted by the activated T cells that infiltrate the brain. Ultimately, activated leukocytes pass through the astrocytic barrier at the GL and thereby enter the CNS to drive lesion formation and clinical relapse. Microglia are involved in the surveillance of the CNS and continuously scan the environment to defend against infectious pathogens.[13] Microglia have also recently been shown to contribute to BBB induction, and the results of two-photon *in vivo*

Received 21 February 2021; accepted 30 August 2021;
https://doi.org/10.1016/j.omtn.2021.08.030.

Correspondence: Wei Zhang, Greater Bay Biomedical Innocenter, Shenzhen Bay Laboratory, Shenzhen, Guangdong Province, China.
E-mail: zhangweispace@163.com
Correspondence: Jun Wan, Greater Bay Biomedical Innocenter, Shenzhen Bay Laboratory, Shenzhen, Guangdong Province, China.
E-mail: wanj@ust.hk

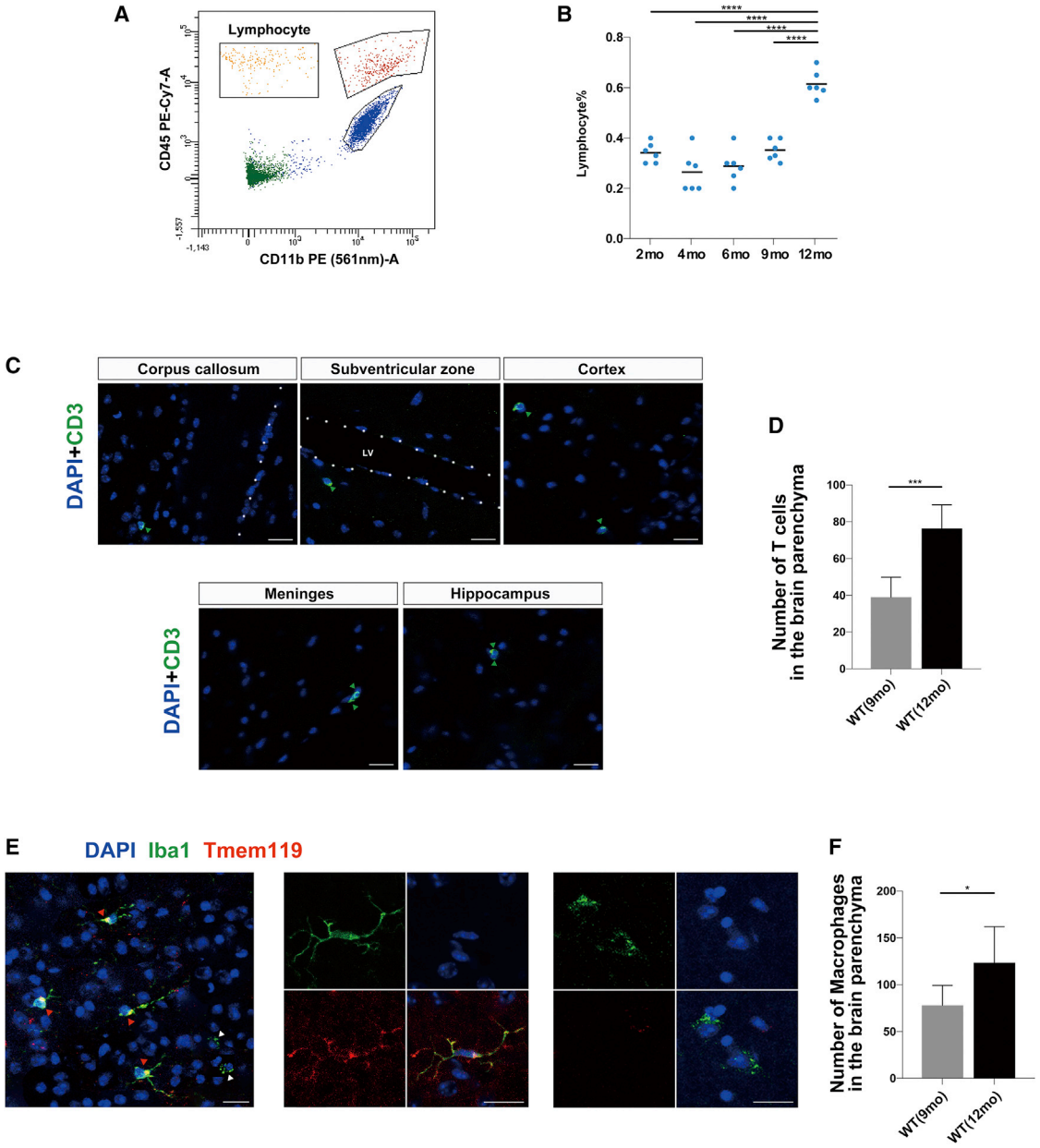

Figure 1. Blood-brain barrier (BBB) permeability to peripheral cells is increased in 12-month-old WT mice

(A) Representative flow-cytometry scattergram showing gating strategy for identification of lymphocyte subsets in brain samples. (B) Quantified percentages of lymphocytes at five time points. (C) Representative epifluorescence images of $CD3^+$ T cells and nucleated cells (DAPI) in corpus callosum, subventricular zone, cortex, meninges, and hippocampus. (D) Total number of $CD3^+$ T cells in 10 brain slices from 9- and 12-month-old WT mice (n = 3). Green arrowheads: T cells. (E) Staining for Iba1 (green) and Tmem119 (red) and DAPI staining (blue) in total brain, and representative epifluorescence images and high-magnification views of ramified microglia ($Iba1^+Tmem119^+$; red arrowheads) and macrophages ($Iba1^+Tmem119^-$; white arrowheads). (F) Total number of $Iba1^+Tmem119^-$ macrophages in 10 brain slices from 9- and 12-month-old WT mice (n = 3). Scale bars represent 20 μm. One-way ANOVA followed by Dunnett post hoc test; data are shown as means ± SEM; unpaired t tests were used for comparing two samples (D and G); ****p < 0.0001, ***p < 0.001, **p < 0.01, *p < 0.05; n = 3 animals.

imaging studies have indicated that microglia also play a dual role in BBB repair. Initially, microglia maintain BBB integrity by expressing the TJ protein Claudin-5 and establishing physical contacts with endothelial cells, but during persistent inflammation, microglia engulf astrocytic endfeet and endothelial cells and impair BBB function. Although these dual roles of microglia and astrocytes have been described, elucidation of precisely how these glial cells change phenotypes when BBB permeability is compromised might help reduce the

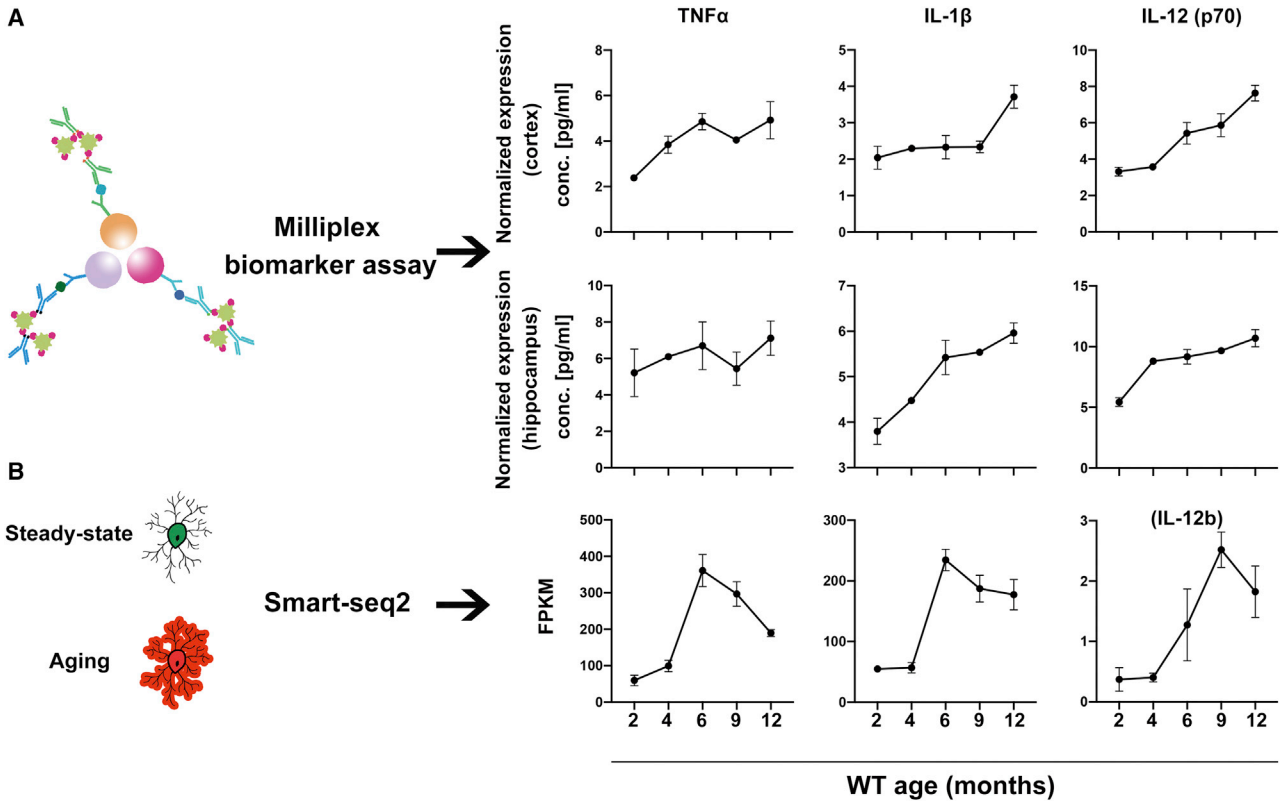

Figure 2. Inconsistency between RNA-seq results and cytokine levels reveal impact of BBB during aging

(A) TNF-α, IL-1β, and IL-12p70 cytokine levels in cortex and hippocampus lysates from five time points in WT mice. (B) RNA-seq analysis of TNF-α, IL-1β, and IL-12p70 expression at five time points in WT microglial samples. Three biological replicates were used for each time point (A and B).

consequent deleterious impact and contribute to recovery of cognitive function.[15]

Here, we investigated the transcriptional changes that occur in microglia and astrocytes by performing RNA sequencing (RNA-seq) on samples from five time points across the BBB permeability change during aging in mice. We report that whereas microglia are characterized by marked gene-level alterations related to negative regulation of protein phosphorylation and phagocytic vesicles, astrocytes show activation of enzyme- or peptidase-inhibitor signaling after detectable changes in BBB permeability. We also identify several genes enriched in these pathways that are notably altered after BBB breakdown. Our data reveal that microglia and astrocytes play an active role in maintaining BBB stabilization and corralling infiltrating cells, and thus might potentially function in ameliorating the lesions and neurologic disabilities in CNS diseases.

RESULTS

Elevated levels of lymphocytes and macrophages in brain

To confirm that aging causes a decrease in BBB integrity, we quantified the percentage of $CD45^{High}$ $CD11b^{-}$ lymphocytes at five time points by using fluorescence-activated cell sorting (FACS) analyses with an appropriate gating strategy (Figure 1A). The percentage of lymphocytes was significantly higher in 12-month-old wild-type (WT) mice than in mice at younger ages (Figure 1B). For further verification, we performed IHC-Fr (Immunohistochemistry frozen sections) on WT mice and quantified the $CD3^{+}$ T cells in total coronal brain sections (Figure 1C). In agreement with our FACS results, T cell numbers in the brain were higher in 12-month-old WT mice than in 9-month-old WT mice (Figure 1D).

We further investigated macrophage levels in the brain of WT mice by staining with antibodies against Tmem119 (a selective marker of resident microglia that does not stain infiltrating macrophages[15–17]) and Iba1 (ionized calcium-binding adaptor molecule 1). Our immunofluorescence analyses revealed that the typical ramified microglia were Tmem119-positive and colocalized with Iba1 immunoreactivity, whereas infiltrating macrophages were $Iba1^{+}/Tmem119^{-}$ (Figure 1E). Notably, quantification (through blinded counting) of $Iba1^{+}/Tmem119^{-}$ macrophages in histologically stained total coronal brain sections revealed increased numbers of the infiltrating macrophages in 12-month-old WT mice (Figure 1F).

Inconsistency between RNA-seq results and cytokine levels

Inflammation plays a critical role in compromising BBB integrity during aging and in neurodegenerative disorders, and upregulation of

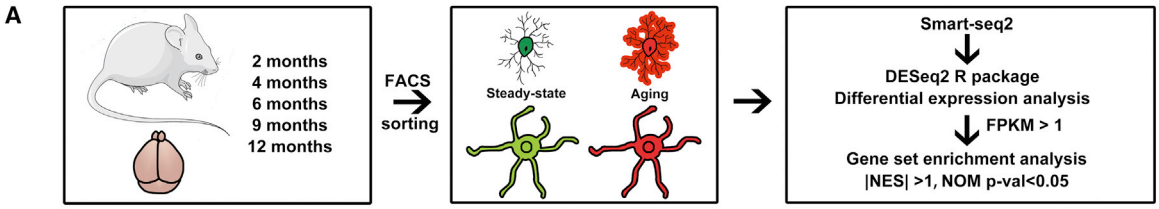

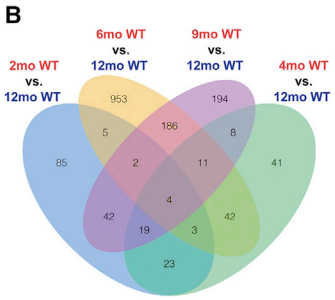

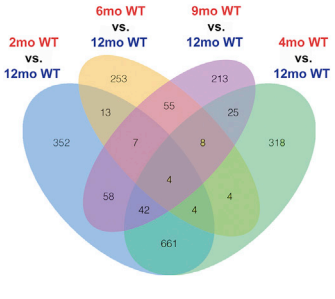

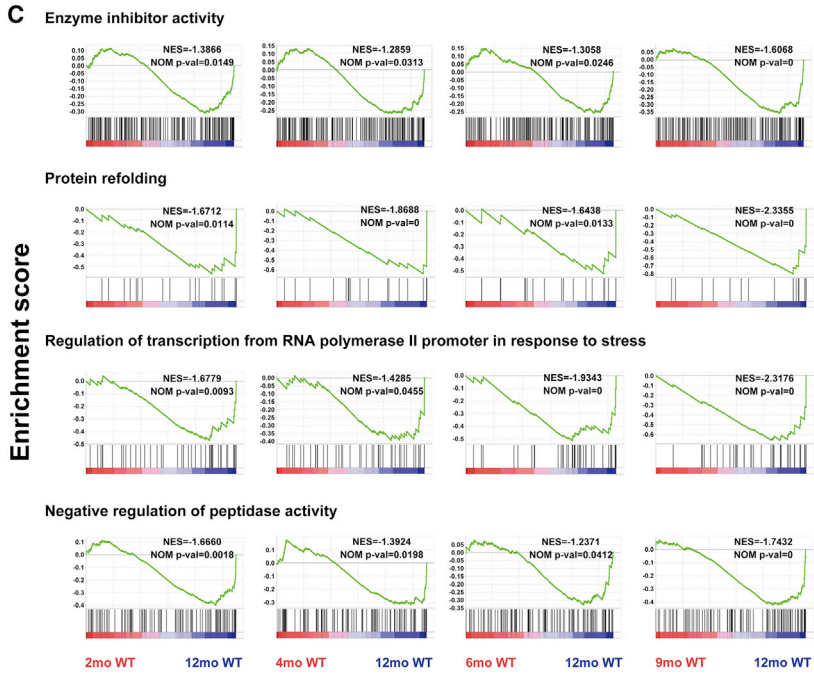

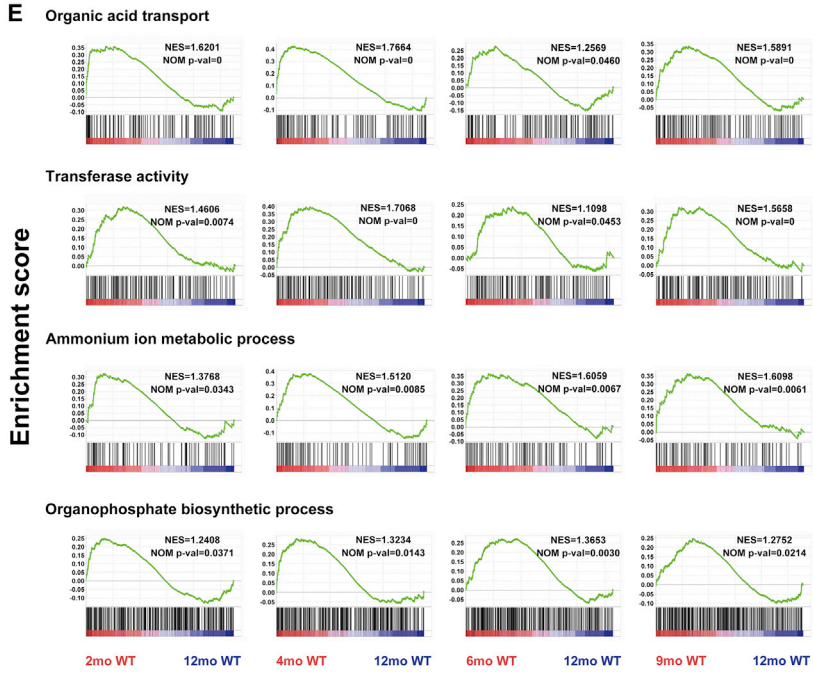

(legend on next page)

ICAM-1 in the presence of proinflammatory mediators such as tumor necrosis factor (TNF)-α, interleukin (IL)-1β, and IL-12 is reported to lead to increased BBB permeability.[18] Therefore, we measured the levels of these proinflammatory cytokines in the hippocampus and cortex lysates of WT mice at five time points; our aim was to ascertain the relationship between inflammatory factors and age-related changes in BBB permeability. TNF-α and IL-1β are mainly secreted by microglia/macrophages and are involved in diverse cellular activities, including cell proliferation, differentiation, and apoptosis. IL-12 is a disulfide-linked heterodimer composed of a 35-kDa subunit encoded by the IL-12a gene and a 40-kDa cytokine receptor-like subunit encoded by the IL-12b gene. IL-12b is expressed by activated macrophages and dendritic cells and exhibits a broad array of biological activities. Here, we observed increased levels of TNF-α, IL-1β, and IL-12p70 from 9-to-12-month-old WT mice (Figure 2A), but our sequencing data indicated that the transcriptome levels of these three factors encoded by microglia were downregulated (Figure 2B). The inconsistency is probably caused by the cytokine secretion from infiltrating peripheral macrophages after BBB dysfunction.

Age-associated functional changes in astrocytes after vascular dysfunction

To investigate the transcriptomic differences between astrocytes before and after BBB destruction, we analyzed our previous sequencing data on astrocytes from mice belonging to five age groups (five time points).[19] We first filtered for genes that are expressed at an appreciable level (FPKM > 1), and then, to identify functional gene sets, we performed gene set enrichment analysis (GSEA) for the enriched genes between the ages at which the BBB was intact (2, 4, 6, or 9 months) and the age at which BBB permeability was increased (12 months) (Figure 3A). As compared with the enriched pathways in 2-month-old astrocytes, the pathways involved in "inner mitochondrial membrane protein complex," "NADH dehydrogenase complex," and "oxidative phosphorylation" were upregulated in 12-month-old astrocytes. Moreover, relative to 4-, 6-, and 9-month-old astrocytes, 12-month-old astrocytes showed upregulation of the following pathways (respectively): "ATPase activator activity" and "peroxidase activity"; "regulatory region DNA binding" and "postsynaptic density"; and "structural constituent of ribosome" and "protein refolding." Table S1 shows the complete datasets. To identify core upregulated pathways, we searched for overlap in enrichment pathway changes between 12-month-old astrocytes and 2-, 4-, 6-, and 9-month-old astrocytes, and we identified these four signaling pathways (Figure 3B): "enzyme inhibitor activity," "negative regulation of peptidase activity," "protein refolding," and "regulation of transcription from RNA polymerase II promoter in response to stress" (Figure 3C). Furthermore, to identify the core pathways that were differentially downregulated, we constructed Venn diagrams of the GSEA results for astrocytes (2-, 4-, 6-, and 9-months-old, relative to 12-months-old; complete datasets in Table S2), which revealed these four signaling pathways (Figure 3D): "organic acid transport," "transferase activity," "ammonium ion metabolic process," and "organophosphate biosynthetic process" (Figure 3E).

We next applied specific filtering criteria (adjusted $p < 0.05$, $|\log2 \text{fold-change}| > 0.5$) to identify genes that were significantly upregulated or downregulated in 12-month-old astrocytes relative to 2-, 4-, 6-, and 9-month-old astrocytes. Cluster analysis of mRNA expression was conducted, and heatmaps were generated (Figure 4A) to reveal the differentially expressed genes (DEGs) in astrocytes (with three replicates used at the five time points). We found that 1,495 genes were upregulated and 1,709 genes were downregulated in 12- versus 2-month-old astrocytes; 504 and 859 genes were upregulated and downregulated respectively in 12- versus 4-month-old astrocytes; 3,925 and 3,024 genes were upregulated and downregulated in 12- versus 6-month-old astrocytes; and 544 and 341 genes were upregulated and downregulated in 12- versus 9-month-old astrocytes (Figure 4B). Relative to 2-, 4-, 6-, and 9-month-old astrocytes exclusively, 32 DEGs were significantly upregulated (Figure 4C) and 37 DEGs were significantly downregulated (Figure 4D) concurrently in 12-month-old astrocytes.

By analyzing the GSEA results, we sought to ascertain which genes contributed to the increased or decreased enrichment of the aforementioned 8 core pathways in 12-month-old astrocytes. However, the expression of certain core enriched genes (as per GSEA) did not show a pronounced age-related change. To identify the potential BBB regulatory genes that are significant altered when BBB permeability is compromised, we next conducted Venn analysis of the core GSEA genes and core DEGs, and our results identified 8 age-upregulated candidate genes (Figure 5A) including *Pcsk1n*, which encodes a protein that functions as an inhibitor of prohormone convertase 1; *Ppp1r14a*, which encodes an inhibitor of smooth muscle myosin phosphatase that enhances smooth muscle contraction;[20–22] and *C4b*, which encodes a component of the complement cascade involved in endopeptidase inhibitor activity that reduces the invasion and adhesion of peripheral pathogens to endothelial cells.[23,24] Among the genes, we also found three genes encoding heat shock proteins, *Hspa1a*, *Hspa1b*, and *Dnajb1* (also known as *Hsp40*), which are protective molecular chaperones that prevent protein aggregation and aberrant intermolecular interactions.[25,26] The heatmap illustrates the expression of the eight genes in astrocytes. Lastly, the overlapping set contained two age-downregulated candidate genes, *Rrm2* and *Dck* (Figure 5B). The relationship between signaling cascades and candidate genes is shown in Figure 5C.

Figure 3. Gene set enrichment analysis (GSEA) to identify potential targets of BBB dysfunction in astrocytes

(A) Transcriptome strategy in RNA-seq performed on microglia and astrocytes. Three biological replicates were used for each time point. (B) Venn diagram of shared pathways among upregulated signaling pathways in astrocytes. (C) GSEA results showing enrichment of core upregulated pathways in different groups. (D) Venn diagram of shared pathways among downregulated signaling pathways in astrocytes. (E) GSEA results showing enrichment of core downregulated pathways in different groups. NES, normalized enrichment score; NOM p-val, nominal p value.

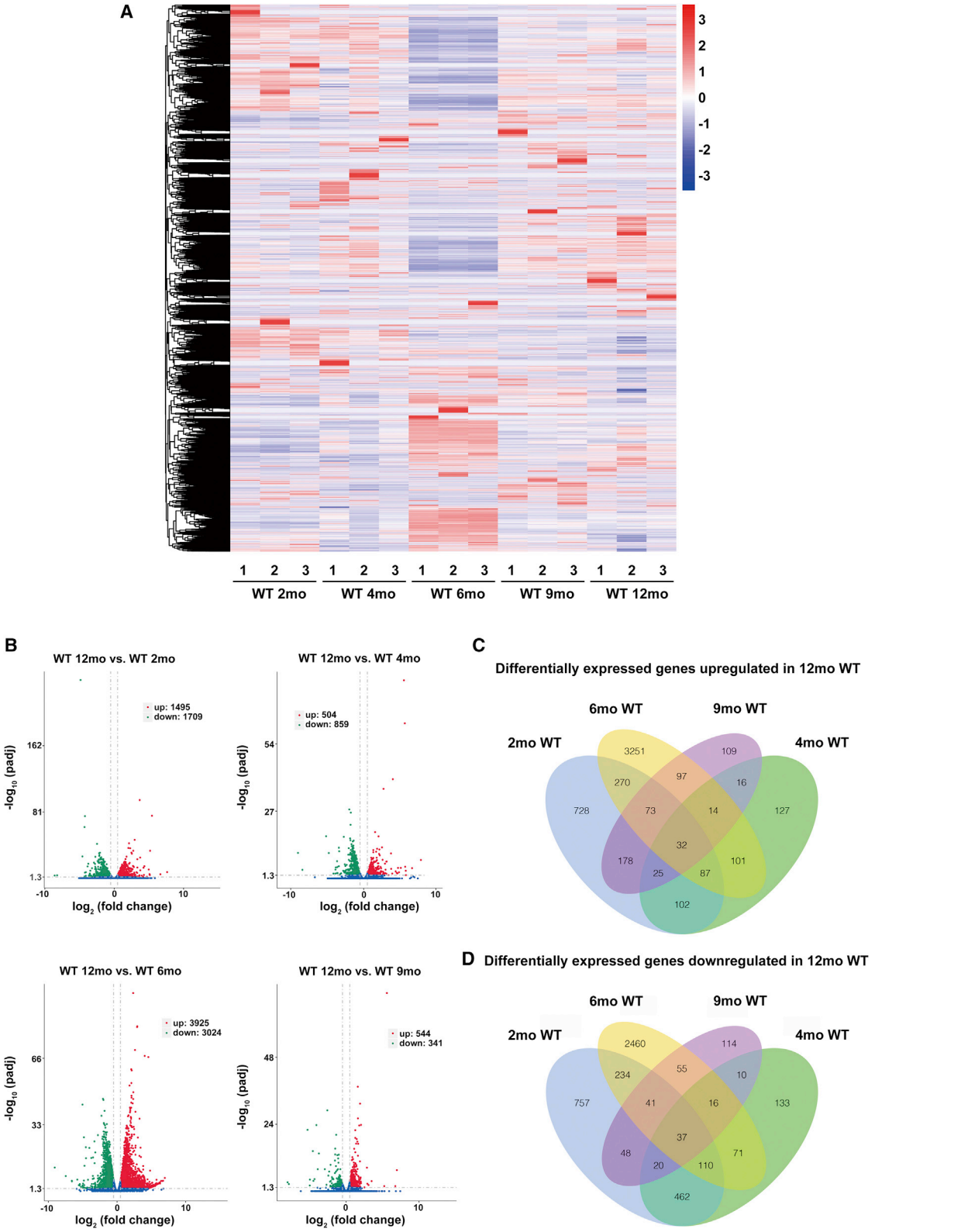

(legend on next page)

Does BBB dysfunction cause microglial dysfunction?

Increasing evidence indicates that resident microglia in the brain parenchyma also play a key role in modulating BBB integrity and function during aging and disease.[27–29] To identify genes that show differential expression profiles in 12-month-old microglia relative to younger microglia (Figure 6A), we again applied specific filtering criteria (adjusted $p < 0.1$, $|\log2 \text{ fold-change}| > 0.5$) and obtained these results: 1,109 genes were DE in 12- versus 2-month-old microglia, with 527 and 582 genes being respectively upregulated and downregulated; 650 genes were DE in 12- versus 4-month-old microglia, with 298 and 352 upregulated and downregulated; 5,868 genes were DE in 12- versus 6-month-old microglia, with 3,208 and 2,660 upregulated and downregulated; and 346 genes were DE in 12- versus 9-month-old microglia, with 164 and 182 upregulated and downregulated (Figure 6B). Of these genes, 18 and 28 were upregulated and downregulated overlapping core genes (Figures 6C and 6D). To characterize the enrichment of functionally related sets of all genes, we used GSEA to identify genes from 12-month-old microglia relative to 2-, 4-, 6-, and 9-month-old microglia, respectively. The complete upregulated and downregulated pathways are shown in Tables S3 and S4. The overlap of the core GSEA results revealed that gene sets related to protein tyrosine/serine/threonine phosphatase activity, negative regulation of stress-activated mitogen-activated protein kinase (MAPK) cascade, and negative regulation of protein phosphorylation were typically upregulated after BBB disruption (Figures 7A–7C); conversely, gene sets related to phagocytic vesicles, phagocytic vesicle membrane, import across plasma membrane, cell surface, negative regulation of leukocyte proliferation, and extracellular space were downregulated (Figures 7D–7I). The core candidate genes that were upregulated and downregulated before and after the BBB permeability change are shown in Figures 7J and 7K, which also includes a Circos diagram generated to visualize the correspondence between enriched pathways and genes (Figure 7L).

Validation of RNA-seq profiles by using qPCR and western blot

To confirm the differential expression of candidate genes identified in our RNA-seq experiments, we performed qPCR and western blot by using a new cohort of animals. For qPCR validation, we selected seven genes each from microglia and astrocytes. Data were expressed as $2^{-\Delta\Delta Ct}$ by using the *Gapdh* transcript as an internal reference standard. These expression analyses performed on the selected genes yielded results that were superimposable with the results obtained using RNA-seq (Figures 8A and 8B). All primers used are listed in Table 1. Differential expression of protein levels of candidate genes was further validated by western blotting in 2-, 9-, and 12-month-old astrocytes (Figures 8C and 8D) and microglia (Figures 8E and 8F). Among the eight selected genes, the protein levels encoded by *Dnajb1*, *Hspa1a*, *Hspa1b*, *Nr4a1*, *Dnaja1*, and *Hsph1* genes showed an increase in 12-month-old cells, which were consistent with the sequencing results, while the protein levels encoded by *Rrm2* and *Dck* genes did not change.

DISCUSSION

BBB dysfunction has been increasingly recognized to contribute to the autoinflammatory conditions of mild cognitive impairment (MCI), multiple sclerosis, and Alzheimer's disease (AD).[30–32] Previous research has revealed multiple cerebral microvascular ultrastructural impairments in APP/PS1 mice[33] and AD postmortem tissue[34] that coexist with cerebral amyloid aggregates and cognitive deficits. Neuroimaging studies in the living human brain have also shown an age-dependent BBB breakdown in the hippocampus, with the BBB integrity being worsened with MCI.[35–37] The endotheliocyte, which is the anatomic unit of the BBB, is the first barrier for the control of leukocyte and soluble-factor entry from the circulation into the brain parenchyma. In healthy adults, the establishment and maintenance of the endothelial barrier depends on astrocytes. Microglia, the active surveyors of the brain parenchyma, respond rapidly to present a range of reactive phenotypes in brain infection and damage and localize in close physical association with microvascular structures; this suggests that microglia play a role both in angiogenesis and in the conferring of BBB properties to the brain microenvironment. The bidirectional crosstalk between these cells maintains the separated pools of neurotransmitters and neuroactive agents that act centrally and peripherally, and this guarantees an appropriate environment for not only enabling proper neural function but also protecting the CNS from injury and disease (Figure 9). In inflammatory lesions, BBB integrity is disrupted, which leads to the penetration of the brain by inflammatory cells, soluble neurotoxic proteins, and pathogens; however, the vascular-derived factors can also induce phenotypic changes in microglia and astrocytes *in vivo* (Figure 9). Our goal in this study was to identify the transcriptomic changes in microglia and astrocytes during their response to peripheral factors and the contribution of this alteration to BBB integrity.

Our results agree with previous findings that T cells appear in the brain at ~12 months of age in mice and that their numbers increase further during aging.[38] Although various cell types can produce and secrete TNF-α, IL-1β, and IL-12, the cytokine secretion is also subject to release from the inflammasome that recognizes danger signals and activates the pro-inflammatory process. Macrophages/microglia are the primary producers of TNFα, IL-1β, and IL-12.[39–41] Therefore, peripheral macrophages may infiltrate the brain and produce pro-inflammatory factors to play a regulatory role after BBB dysfunction.

Here, by analyzing gene expression after BBB breakdown, we found that astrocytes appear to function as enzyme inhibitors, which suggests that activated astrocytes not only upregulate TJ proteins to close the GL and restrict leukocyte entry into the perivascular space[13] but also

Figure 4. Transcriptomic profiles of astrocytes at five time points

(A) Heatmap and hierarchical clustering of normalized read counts from astrocytes, normalized by row mean. (B) Upregulated and downregulated genes determined using DESeq2 analysis, between 2-, 4-, 6-, and 9-month-old mice and 12-month-old mice; adjusted $p < 0.05$, |log2 fold-change| > 0.5. (C) Venn diagram showing upregulated genes in astrocytes. (D) Venn diagram showing downregulated genes in astrocytes.

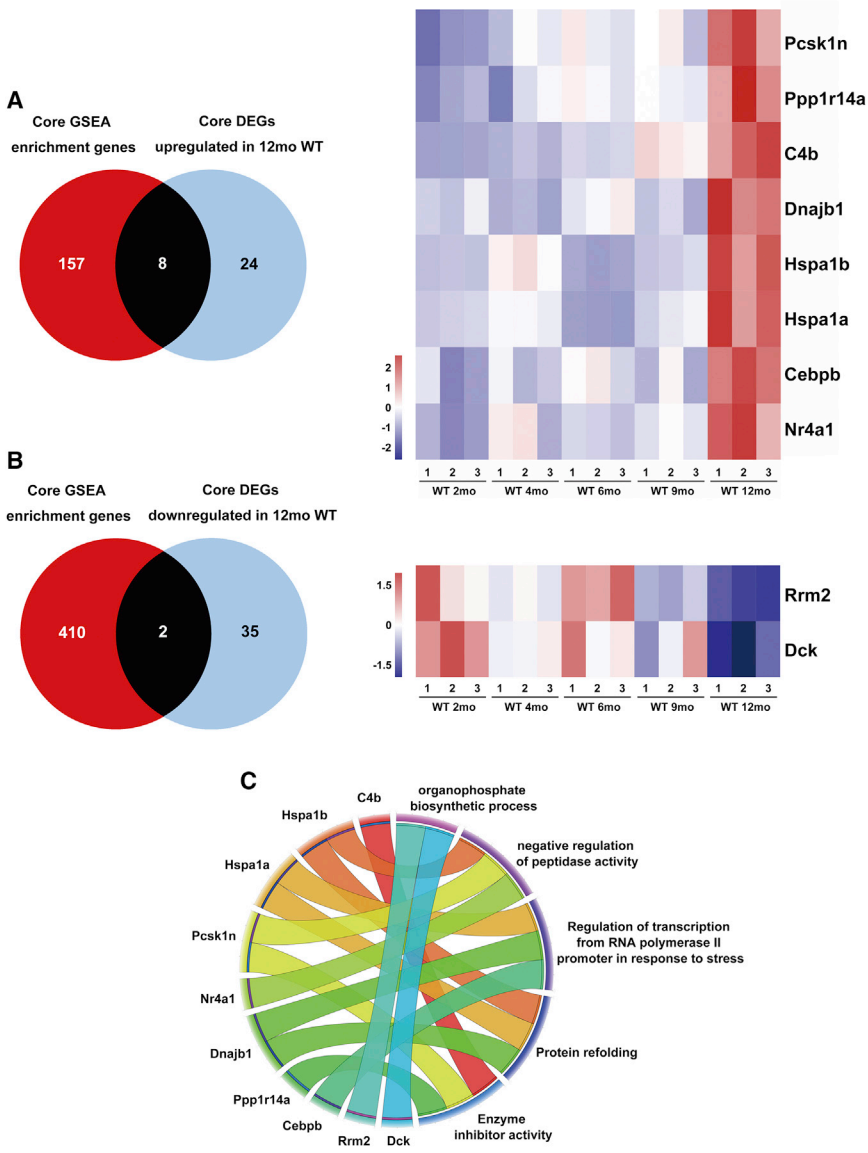

Figure 5. Transcriptome RNA-seq for confirming core genes associated with BBB dysfunction in astrocytes

(A) Analysis of co-occurrence between core genes that account for increased gene set enrichment signal and genes that are significantly upregulated during BBB dysfunction. (B) Analysis of co-occurrence between core genes that account for decreased gene set enrichment signal and genes that are significantly downregulated during BBB dysfunction. (C) Correspondence between pathways and candidate genes.

upregulate protease inhibitors to protect against the degradative enzyme secreted by the infiltrating lymphocytes. *ProSAAS*, encoded by gene *Pcsk1n*, an abundant secretory polypeptide that is widely expressed in the human, mouse, and rat brain, regulates the proteolytic cleavage of neuroendocrine peptide precursors. *ProSAAS* has been widely suggested to colocalize with Lewy bodies or amyloid plaques and carry out chaperone anti-aggregant functions in AD, Pick's disease, and Parkinsonism-dementia (Figure 10),[42–47] contribute to the physiological effects of psychostimulants,[48] and serve as a therapeutic agent in the case of food-intake disorders[49,50] as well as a cerebrospinal fluid biomarker in AD and frontotemporal dementia.[51,52] It has been previously reported that *Pcsk1n* expression was upregulated in the hippocampus of rats with more severe BBB disruption;[53] however, the role of ProSAAS in BBB regulation in mice has remained obscure. *Ppp1r14a* (also known as *CPI-17*) encodes one of the limited numbers of DE protein, shown to regulate cerebral circulation or exert vasomotor effects on cerebral arteries.[54] Endogenous CPI-17 is involved in controlling endothelial cell motility.[55] These indicate that astrocytes could secrete neuronal mediators of vasoactivity to regulate cerebral vasoconstriction in healthy aging as well as in pathologic conditions, such as in cerebrovascular and neurodegenerative diseases. Among the eight age-upregulated candidate astrocyte genes, *Nr4a1* and *Cebpb* can both be potentially induced in vascular inflammation or pathologies. Nr4a1, a member of the Nur nuclear-receptor family of transcription factors, has been shown to attenuate the neuroinflammatory response by regulating NF-κB and thus preserve BBB integrity after experimental intracerebral hemorrhage.[56–58] The protein encoded by *Cebpb* not only binds to CLDN4 promoter[59] but also functions as the key transcription factor that regulates the promoter region of MALAT1, which protects cerebrovascular endothelial cells against inflammatory responses and maintains BBB integrity after stroke.[60] Cebpb can also bind to Nr4a1 promoter[61] or enhancer elements and induce Nr4a1 expression.[62] Hspa1a and Hspa1b are two major orchestrators of the cellular stress response and encoding proteins that belong to the Hsp70 family (heat shock protein family A) member proteins. In response to various exogenous stresses, astrocytes activate heat-shock response to attenuate the accumulation of denatured cytoplasmic proteins known to restore the normal ability to maintain the BBB function.[63]

Bradykinin, histamine, 5-hydroxytryptamine, and substance P acting on astrocytes can lead to the formation of ATP and prostaglandins, and this enhances endothelial permeability. Astrocytes downregulate "organic acid transport," "ammonium ion metabolic," and "organophosphate biosynthetic" pathways and thus exclude the inflow of potentially harmful compounds through the "physical barrier."

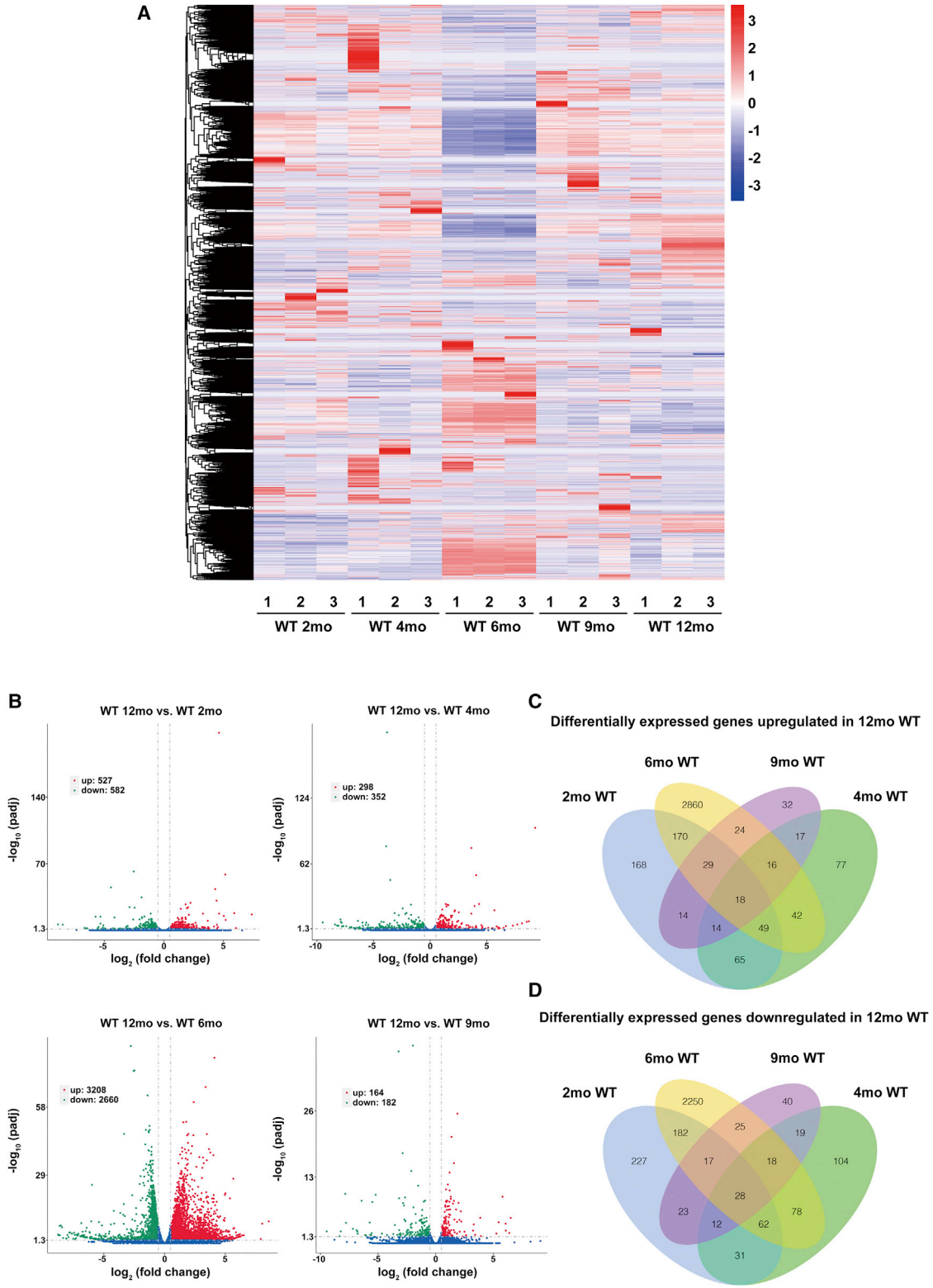

(legend on next page)

Collectively, these data suggest that astrocytes function as "facilitators" in vascular recuperation after injury or inflammation. The identified astrocyte gene sets may potentially serve as novel therapeutic targets. Dnaja1 and Dnajb1, which belong to heat shock protein family Hsp40, are cofactors that stimulate the ATPase activity of Hsp70 in order to promote protein folding and prevent misfolded protein aggregation.[64] To estimate whether the BBB dysfunction-related changed genes are involved in human diseases, we compared our gene sets to the human disease-associated genes reported previously. We found that *Dnajb1*, *Hspa1a*, and *Hspa1b* were also significantly upregulated in the single-nucleus sequencing data of astrocytes in AD patients.[65] *C4B* is associated with systemic lupus erythematosus,[66] diabetes,[67] and autism[68] and also increased in AD patients.[69] *NR4A1* has recently emerged as a therapeutic target for aging,[70] steroidogenesis,[71] inflammation,[72] and oncogenesis.[73] CPI-17 is implicated in the etiology of asthma and inflammatory bowel diseases.[74,75] *RRM2* was overexpressed in breast, pancreatic, gallbladder, and liver cancer patients.[76] The high expression level of *Dck* was found in patients with liver cancer.[77] High expression levels of C5ar1 receptors were found in blood and pulmonary myeloid cells of COVID-19 patients (Figure 10).[78] Histamine and Rho kinases (RhoK, serine/threonine kinases) can directly increase the phosphorylation of occludin and other TJ proteins.[79,80] Conversely, dominant-negative RhoK and RhoK inhibitors reduce occludin phosphorylation and migration of monocytes through the BBB.[81] In response to stress, MAPKs can be activated,[82] and deregulated MAPK activation is frequently detected in diseases, including various cancers and inflammatory and neuronal diseases. Previously, stable transfection of cells with constitutively active MAPKs was shown to reduce the tyrosine phosphorylation of occludin and weaken the BBB.[83–85] The transcriptome GSEA results here confirmed that microglia negatively regulated tyrosine/serine phosphatase and MAPK activation to reduce monocyte transmigration, and that, concurrently, the phagocytotic action of microglia toward astrocytic endfeet and endothelial cells was downregulated, which also contributed to the further recovery of BBB integrity. The therapeutic targets that reduce the infiltration and infringement of peripheral substances or pathogens into the CNS or reduce damage to factors beneficial to protecting the BBB hold great potential to treat chronic neurological diseases and acute CNS injuries.

In the case of most neurodegenerative disorders, the early steps in the disease processes remain unclear, and biomarkers for these stages have not yet been identified. Our data reveal how microglia and astrocytes change their phenotypes when BBB permeability is compromised: both transform into cells featuring a reactive phenotype to ameliorate BBB dysfunction and protect BBB integrity. We also identified certain candidate molecules and signaling pathways involved in the transformation during early aging, and this could potentially facilitate the development of new therapeutic strategies for reversing BBB dysfunction and reducing neural damage in chronic neurodegeneration.

MATERIALS AND METHODS

Mice

C57BL/6J WT mice, obtained from the Model Animal Research Center of Nanjing University (Nanjing, China), were originated from The Jackson Laboratory. Mice (n = 3/group) were bred under SPF (Specific pathogen-free) conditions in IVC (Individually ventilated caging) cages at 23°C and 50%–60% humidity and with circadian-rhythm illumination. Pups aged 21 to 28 days old were removed from their parental cages. All procedures were approved by the Animal Use and Care Committee of Shenzhen Peking University - The Hong Kong University of Science and Technology Medical Center (SPHMC) (protocol number 2011-004). All mice used in the study were males. Efforts were made to minimize suffering and the number of animals used.

Immunohistochemistry and image quantification

Mice were deeply anesthetized using pentobarbital, transcardially perfused with ice-cold PBS until the irrigation fluid was completely clear, and then perfused with ice-cold 4% paraformaldehyde (PFA) for 10 min. Brains and spleens were removed, post-fixed in 4% PFA in a 4°C refrigerator for 12 h, dehydrated using a sucrose dilution series, embedded in molds containing Tissue-Tek OCT, and frozen in dry ice. The OCT-embedded brain and spleen samples were cut into 16-μm coronal sections that were placed onto Fisherbrand Superfrost Plus microscope slides (12-550-15; Thermo Fisher Scientific). After blocking and permeabilization for 1 h in PBS containing 4% bovine serum albumin (BSA) and 0.4% Triton X-100, the slices were incubated at 4°C overnight with primary antibodies diluted in PBS, washed with PBS, and incubated with secondary antibodies in PBS at room temperature for 2 h. Nuclei were visualized using 4′,6-diamidino-2-phenylindole (DAPI). Images were captured as z stacks by using a Zeiss LSM710 confocal microscope (Carl Zeiss) with a 20× objective (NA 0.8) or a 63× oil-immersion objective (NA 1.4), and then maximum-intensity projections were obtained. Lastly, blinded counting was used to quantify single-positive and double-positive cells. All parameters were maintained constant between images to allow unbiased detection. The following antibodies were used for staining: anti-IBA1 (019-19741, Wako; 1:300); anti-TMEM119 (400-011, Synaptic Systems; 1:100); anti-CD3 (ab5690, Abcam; 1:100); donkey anti-rabbit Alexa Fluor 488 (A11001, Invitrogen; 1:500); and goat anti-mouse Alexa Fluor 555 (A21422, Invitrogen; 1:500).

Cytokine level detection by using Milliplex kits

Under deep anesthesia, mice were transcardially perfused with ice-cold PBS until the irrigation fluid was completely clear. After decapitation, the brains were removed, and the hippocampus and cortex

Figure 6. Transcriptomic profiles of microglia at five time points

(A) Heatmap and hierarchical clustering of normalized read counts from microglia, normalized by row mean. (B) Upregulated and downregulated genes determined using DESeq2 analysis, between 2-, 4-, 6-, and 9-month-old mice and 12-month-old mice; adjusted $p < 0.05$, |log2 fold-change| > 0.5. (C) Venn diagram showing upregulated genes in microglia. (D) Venn diagram showing downregulated genes in microglia.

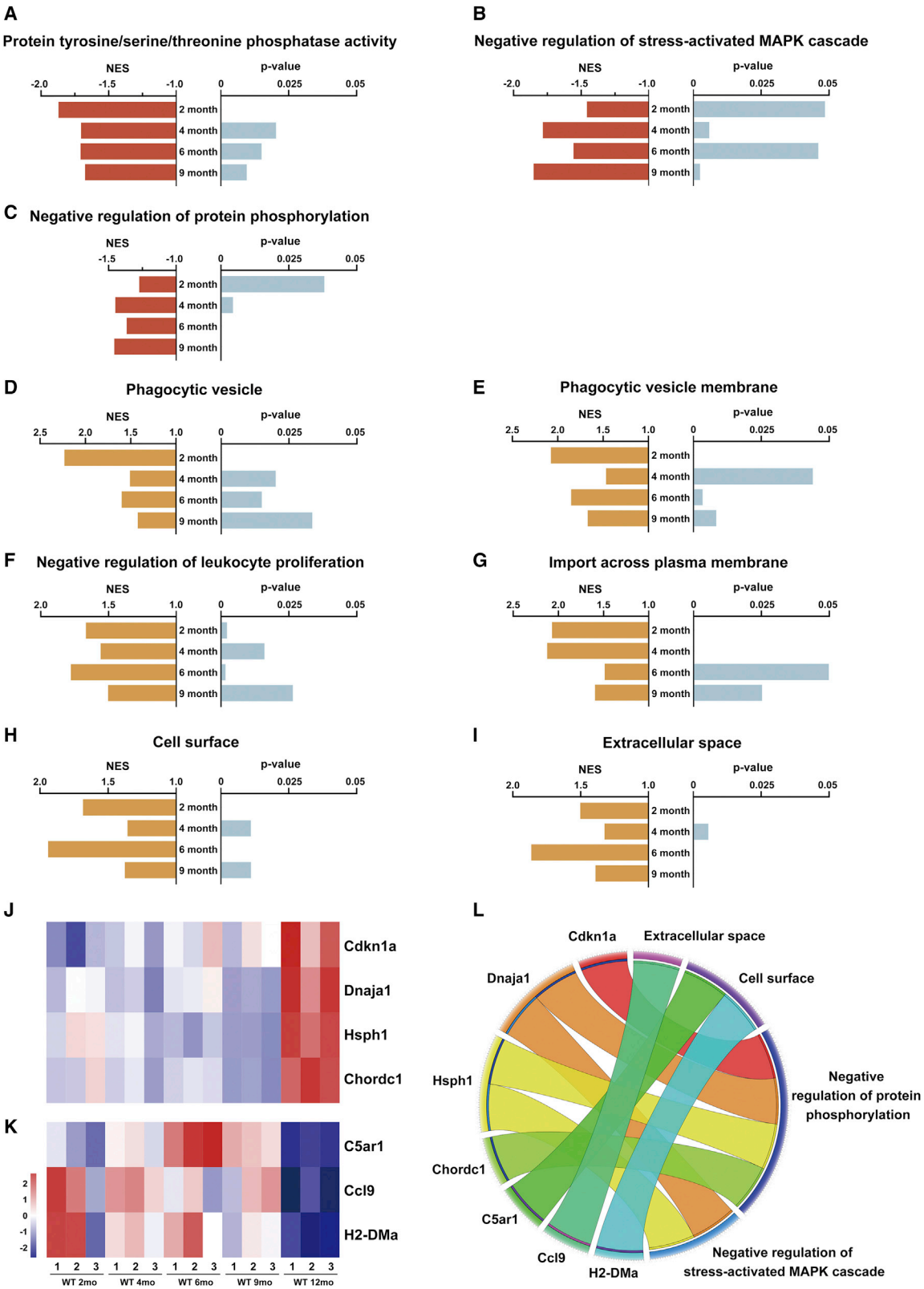

(legend on next page)

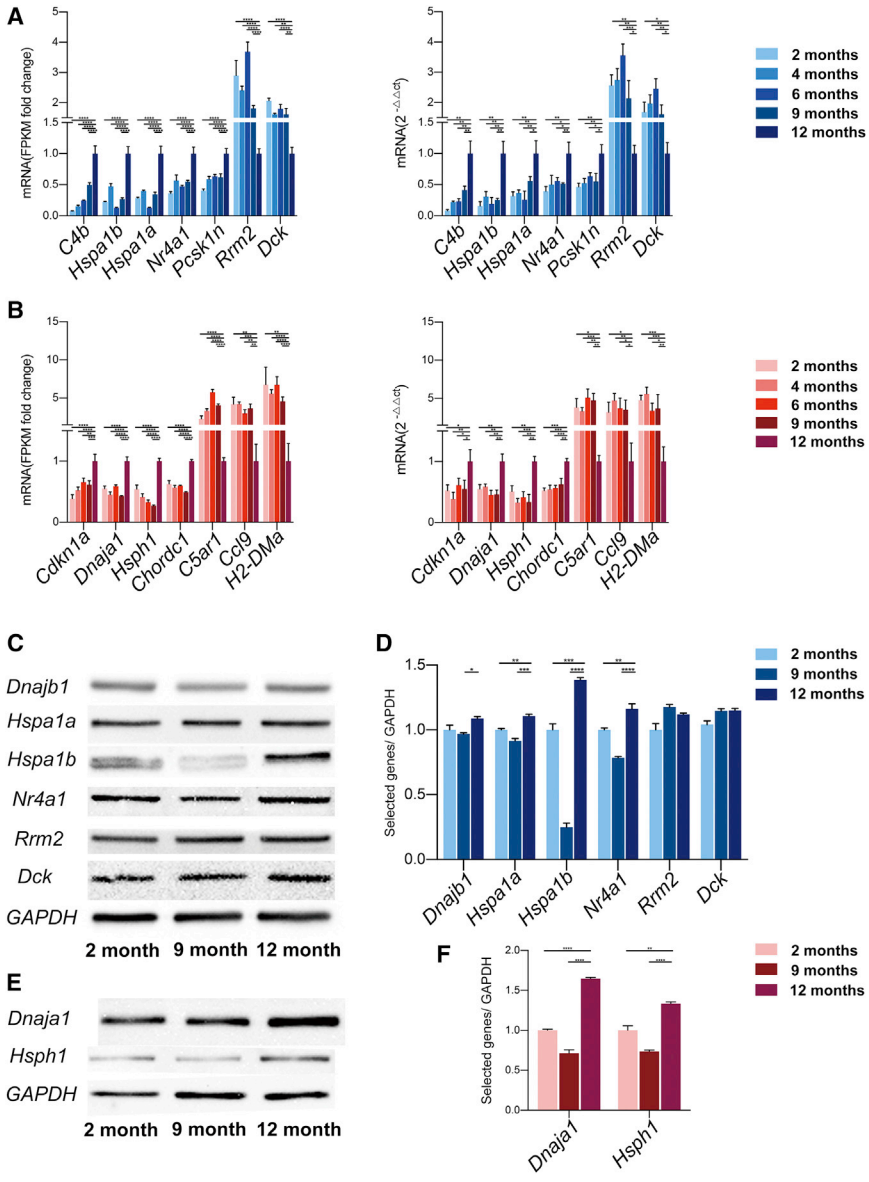

Figure 8. Validation of transcriptome data by using qPCR and western blot (WB)

(A and B) Expression analyses performed on selected genes yielded results superimposable with results obtained from RNA-seq analyses of (A) astrocytes and (B) microglia. Left: comparisons of DESeq2-analysis values between 12-month-olkd samples and 2-, 4-, 6-, and 9-month-old samples. Right: unpaired t tests for comparing two samples. (C) WB analysis of selected genes in astrocytic lysates. Loading was quantified by blotting with an anti-GAPDH antibody in cell lysates. (D) Quantification of the blot in (C) (unpaired t tests for comparing two samples). (E) WB analysis of selected genes in microglial lysates. Loading was quantified by blotting with an anti-GAPDH antibody in cell lysates. (F) Quantification of the blot in (E) (unpaired t tests for comparing two samples). Columns represent means ± SEM; ****$p < 0.0001$, ***$p < 0.001$, **$p < 0.01$, *$p < 0.05$.

were micro-dissected on ice in Hank's balanced salt solution (HBSS) and the meninges were removed. The cell lysis buffer from CST (9803) was diluted with ddH_2O, and 1 mM protease-inhibitor cocktail (set III, EDTA-Free; 539134, Millipore) was added before use; tissues were extracted at a ratio of 100 mg of tissue to 1 mL of buffer, homogenized, and spun for 10 min at 14000 × *g* at 4°C to remove precipitates. Duplicate samples of the supernatant were collected for quantifying total protein concentrations by using Bradford protein assay. Each sample was analyzed for cytokines by using a MCYTOMAG-70K Mouse Cytokine magnetic kit (EMD Millipore, Billerica, MA, USA), and data were analyzed using Milliplex Analyst 5.1 software (EMD Millipore). Measurements were corrected for noise by subtracting the average of two technical control wells for each secreted soluble factor.

Brain dissociation

Microglia and astrocytes were isolated from WT mice that were 2, 4, 6, 9, or 12 months old (five groups, 2- to 12 months old). Mice were transcardially perfused under deep anesthesia with 1 × PBS, and then the brain was removed, dissected, and rinsed in HBSS. Next, after removing the meninges, the brain was cut into small pieces by using a sterile scalpel, and the samples were centrifuged at 300 × *g* for 2 min at room temperature, and the supernatant was aspirated carefully. Samples from a single brain were pooled as a single experimental group. Enzymatic cell dissociation was performed using an Adult Brain Dissociation Kit (130-107-677, Miltenyi Biotec) according to the manufacturer's instructions. Briefly, tissue pieces (up to 500 mg of tissue per sample) were transferred into the C Tube containing

Figure 7. Effects on microglial genes in BBB dysfunction

(A and B) GSEA showing enrichment distribution for genes between 2-, 4-, 6-, 9-month old WT and 12-month-old WT in microglial samples. Significantly upregulated (A) and downregulated (B) pathways in 12-month-old samples are identified. (C) Analysis of co-occurrence between core genes that account for increased gene set enrichment signal and genes that are significantly upregulated during BBB dysfunction. (D) Analysis of co-occurrence between core genes that account for decreased gene set enrichment signal and genes that are significantly downregulated during BBB dysfunction. (E) Correspondence between pathways and candidate genes.

Table 1. Primers used in this study

Name	F/R	Primer (5′ to 3′)
C4b	forward	GCAGCCTGTTTCCAGCTCAA
	reverse	CCCTGTAGAGCAGAGCCTCTAA
Hspa1b	forward	TTGATAGCTGCTTGGGCACC
	reverse	CTTCCCAGGCTACTGGAACA
Hspa1a	forward	GCACGTGGGCTTTATCTTCC
	reverse	GTCCTACAGTGCAACCACCA
Nr4a1	forward	GAAAGTTGGGGGAGTGTGCTA
	reverse	GGTGTCAAACTCTCCGGTGT
Pcsk1n	forward	GCTGCTGTGCCTAATACCCA
	reverse	GGAGTGCTCGTCTCAACCAA
Rrm2	forward	TGATGCCGGGCCTTACATTT
	reverse	ATAAGCCTGTCGGCCACAAA
Dck	forward	AACGTCTCAGAAGAGCGGTG
	reverse	CCAGTCGTGCCAGTCTTGAT
Cdkn1a	forward	GAATTGGAGTCAGGCGCAGA
	reverse	AAAGTTCCACCGTTCTCGGG
Dnaja1	forward	CGGGGCTCGGCTACAAAA
	reverse	TGCTCCGCCCTCTTTAATCG
Hsph1	forward	GAGGCGCCGGTGAGTAAAAT
	reverse	GAGCCTACGTCTAGCCCAAC
Chordc1	forward	TGCTGCGGTGATTCACTTCT
	reverse	ACCTGGGTGGTATGTGCAAG
C5ar1	forward	GAGCACCTCCAGGAGACAAG
	reverse	ATTCCCAGGTACTCCCACCA
Ccl9	forward	TCGGTTTCCCAGCGGATTTT
	reverse	GGCTTACTGATGGAGGGGTG
H2-DMa	forward	CATGCTGTGGTCCCAGGAG
	reverse	GTAGCTGCCTGGCTCTTCAA

1950 µL of enzyme mix 1 (Enzyme P and Buffer Z), and then 30 µL of enzyme mix 2 (Enzyme A and Buffer Y) was added into the C Tube. The C Tube was tightly closed and attached upside down onto the sleeve of the gentleMACS Octo Dissociator with Heaters (130-096-427, Miltenyi Biotec), and the appropriate gentleMACS program was run. After brief centrifugation to collect samples at the tube bottom, the samples were filtered through a 70-µm strainer (130-098-462, Miltenyi Biotec), washed with D-PBS, and then centrifuged again.

Percoll density gradient and myelin removal

Single cells were resuspended in 40% Percoll and centrifuged at 800 × *g* for 20 min at 15°C. After discarding the myelin-containing supernatant, the pellet was resuspended in cold MACS buffer (containing 1-volume dilution of PBS, 2 mM EDTA, 0.5% BSA, pH 7.2), and then myelin-removal beads (Myelin Removal Beads II, 130-96-733, Miltenyi Biotec) were used according to the manufacturer's protocol to prepare cells for staining with FACS antibodies. Briefly, single-cell suspensions were incubated with the beads at 4°C for 15 min, and then the cells were washed onto the LS column on the autoMACS Separator; the column was washed thrice with MACS buffer, and the cells in the flow-through were used for antibody staining.

FACS analysis of lymphocytes and FACS sorting of microglia and astrocytes

After isolation, cell pellets were resuspended in FC-receptor-blocking solution (553141, BD Biosciences), incubated on ice for 10 min, and costained for 30 min on ice in the dark with PE-Cy7-labeled CD45 (103114, BioLegend), PE-labeled CD11b (101208, BioLegend), and APC-labeled ACSA2 (130-117-386, Miltenyi Biotec) antibodies. The cells were then rinsed in PBS, centrifuged, resuspended in FACS buffer (1% FBS + 2 mM EDTA, 25 mM HEPES, 1:500 RNase inhibitor in PBS), and incubated in 7AAD (420403, BioLegend) for 10 min before sorting. Data were analyzed using BD FACS Diva v8.0.1 software. Sorted cells were centrifuged at 400 × *g* for 10 min, and pellets were lysed in RLT-buffer (74004, QIAGEN) for RNA extraction.

RNA extraction, quantification, and qualification

RNA was isolated from flow-cytometry-sorted cell populations by using the RNeasy Micro Kit from QIAGEN (74004) according to the manufacturer's instructions, which included a step involving incubation with DNase. For whole-brain RNA purification, we generated 1 brain/pool samples. Purified RNA was quantified using a NanoDrop 2000 (Thermo Scientific) and Agilent Technologies Bioanalyzer 2100 RNA Pico chips (5067-1513, Agilent Technologies) according to manufacturer instructions; the RNA integrity number (RIN) in all cases was >9.

Preparation of SMART-seq2 RNA-seq libraries, sequencing, and data analysis

For RNA sample preparations, 10 ng of RNA per sample was used as the input material. Libraries were generated using a SMART-Seq v4 Ultra Low Input RNA Kit (634892, Takara Bio USA, Mountain View, CA, USA) following the manufacturer's recommendations, and index codes were added to attribute sequences to each sample. Briefly, first-strand cDNA synthesis from total RNA was primed using 3′ SMART-Seq CDS Primer II A, and SMART-Seq v4 Oligonucleotide was used for template switching at the 5′ end of the transcript. PCR Primer II A was used to amplify cDNA, for eight cycles, from the SMART sequences introduced by 3′ SMART-Seq CDS Primer II A and SMART-Seq v4 Oligonucleotide. LD-PCR-amplified cDNA was purified through immobilization on AMPure XP beads and then quantified using the Agilent Bioanalyzer 2100 system. To prepare cDNA libraries suitable for Illumina sequencing, ∼200 pg of cDNA was used with a Nextera XT DNA Library Preparation Kit (FC-131-1024 and FC-131-1096, Illumina, San Diego, CA, USA). Tagmented fragments were amplified for twelve cycles, and dual indexes were added to each well to uniquely label each library. Concentrations were assessed using a KAPA Library Quantification Kit (KK4844, KAPA Biosystems, USA), and samples were diluted to ∼2 nM and pooled. Pooled libraries were sequenced on an Illumina NovaSeq platform and 150-bp paired-end reads were generated. Feature

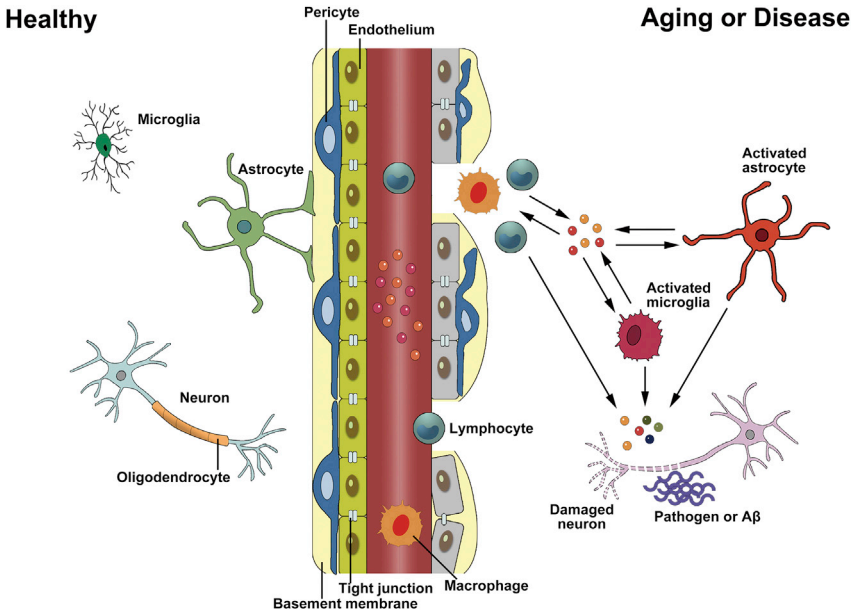

Figure 9. Schematic representation of potential roles of microglia and astrocytes in BBB maintenance

The normal (healthy) capillary features an intact BBB that is composed of tightly joined endothelial cells and supported by mural pericytes, astrocytes, and microglia. Normal aging and neurodegenerative disease are accompanied by increased BBB permeability. The basement membrane is damaged and thickened, pericytes degenerate and detach, and blood-derived molecules and peripheral cells leak from vessels and are directly toxic to neurons and glial cells. The presence of neurotoxic molecules can further exacerbate the ongoing of BBB damage in the CNS. Bidirectional induction of glial targeting factors is necessary to establish and maintain the BBB.

Counts v1.5.0-p3 was used to determine the number of reads mapped to each gene, after which each gene's FPKM (expected number of fragments per kilobase of transcript sequence per million base pairs sequenced) was calculated based on the length of the gene and the number of reads mapped to the gene. Differential expression analysis was performed using DESeq2 R package (1.16.1). GSEA was used to analyze the enriched signaling pathways. Each gene set was permuted 1,000 times to calculate the p value and NES (normalized enrichment score).

Quantitative RT-PCR validation of selected genes

Flow-cytometry-sorted microglia and astrocytes were used for RNA extraction (see preceding sections on FACS and RNA extraction), and quantitative RT-PCR was performed in triplicate in 96-well plates by using a qPCR machine (LC480, Roche) and SYBR Green I Master mixture (4887352001, Roche) to detect amplification products generated using the following thermocycling protocol: initial denaturation at 95°C for 10 min followed by 40

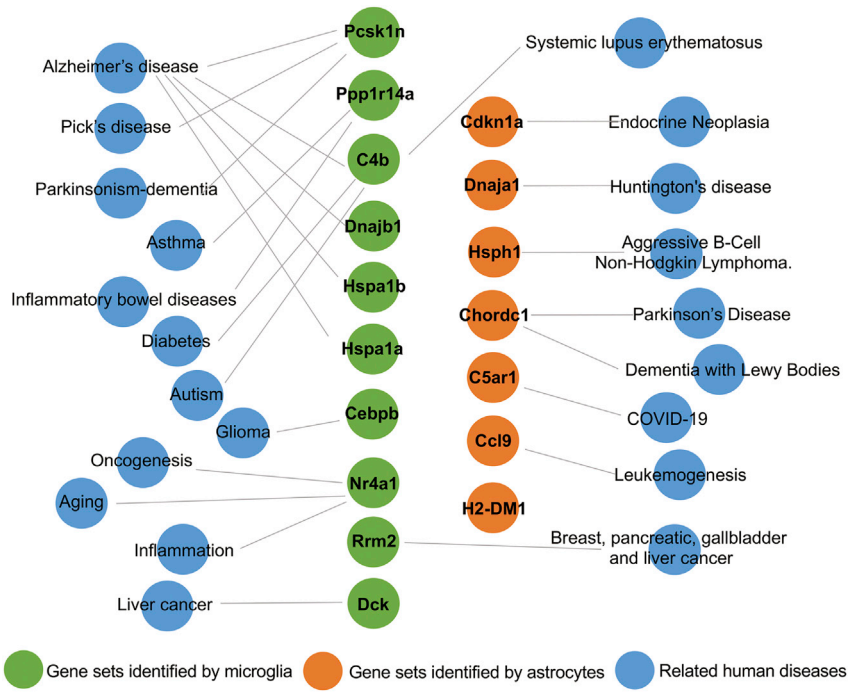

Figure 10. The gene sets identified are involved in human diseases

amplification cycles of 95°C for 15 s and 60°C for 1 min, and a final cycle at 25°C for 15 s. Relative quantification of mRNA expression was performed using the comparative cycle method to obtain this ratio: gene of interest/*Gapdh*. Relative quantification of gene-expression levels was performed using the $2^{-\Delta\Delta Ct}$ method. All primers were designed using NCBI Primer-BLAST; we designed primers to be ~200-bp long.

Western blotting

After FACS sorting, microglia and astrocytes were lysed in cell lysis buffer from CST (9803) in the presence of 1 mM protease-inhibitor cocktail (set III, EDTA-Free; 539134, Millipore) for protein extraction. Duplicate samples of the supernatant were collected for quantifying total protein concentrations by using Bradford protein assay. Samples were separated on 10% SDS-PAGE and then transferred to PVDF membranes. Membranes were blocked with 5% skimmed milk in tris-buffered saline tween (TBST) and incubated with primary antibodies at 4°C overnight and then washed and incubated with horseradish peroxidase (HRP)-conjugated secondary antibodies for 1 h at room temperature. Finally, membranes were visualized with ECL substrate (Millipore). The following antibodies were used for western blot: rabbit anti-DNAJA1 (Proteintech, 11713-1-AP); rabbit anti-DNAJB1 (Proteintech, 13174-1-AP); rabbit anti-HSPH1 (Proteintech, 13383-1-AP); rabbit anti-RRM2 (Invitrogen, PA5-79937); rabbit anti-HSPA1A (Invitrogen, PA5-34772); rabbit anti-HSPA1B (Invitrogen, PA5-97846); mouse anti-dCK (Santa Cruz Biotechnology, sc-393099); mouse anti-Nr4a1 (Santa Cruz Biotechnology, sc-365113); and rabbit anti-GAPDH (Cell Signaling Technology, 2118S).

Statistical analyses

All statistical analyses were performed using GraphPad Prism 8.00 software (GraphPad Software, La Jolla, CA, USA). Most data were analyzed using one-way ANOVA followed by the Dunnett post hoc test for comparisons of >3 samples, and two-sample unpaired t tests were used for comparing two samples. $p < 0.05$ was considered statistically significant.

SUPPLEMENTAL INFORMATION

Supplemental information can be found online at https://doi.org/10.1016/j.omtn.2021.08.030.

ACKNOWLEDGMENTS

We thank the Shenzhen Biomedical Research Support Platform and the Shenzhen Molecular Diagnostic Platform of Dermatology for technical help. This work was supported by National Natural Scientific Foundation of China Grant 82071586 and National Key R&D Program of China Grant 2019YFA0508402.

AUTHOR CONTRIBUTIONS

J.W., W.Z., and J.P. initiated the research; J.P. and J.Z. performed the experiments; J.P., N.M., and B.Y. analyzed the data; J.P., J.W., and W.Z. wrote the paper. All authors read and approved the final manuscript.

DECLARATION OF INTERESTS

The authors declare no competing interests.

REFERENCES

1. Zlokovic, B.V. (2011). Neurovascular pathways to neurodegeneration in Alzheimer's disease and other disorders. Nat. Rev. Neurosci. *12*, 723–738.
2. Zlokovic, B.V. (2008). The blood-brain barrier in health and chronic neurodegenerative disorders. Neuron *57*, 178–201.
3. Sweeney, M.D., Zhao, Z., Montagne, A., Nelson, A.R., and Zlokovic, B.V. (2019). Blood-Brain Barrier: From Physiology to Disease and Back. Physiol. Rev. *99*, 21–78.
4. Saint-Pol, J., Gosselet, F., Duban-Deweer, S., Pottiez, G., and Karamanos, Y. (2020). Targeting and Crossing the Blood-Brain Barrier with Extracellular Vesicles. Cells *9*, 851.
5. Abbott, N.J., Rönnbäck, L., and Hansson, E. (2006). Astrocyte-endothelial interactions at the blood-brain barrier. Nat. Rev. Neurosci. *7*, 41–53.
6. Alvarez, J.I., Dodelet-Devillers, A., Kebir, H., Ifergan, I., Fabre, P.J., Terouz, S., Sabbagh, M., Wosik, K., Bourbonnière, L., Bernard, M., et al. (2011). The Hedgehog pathway promotes blood-brain barrier integrity and CNS immune quiescence. Science *334*, 1727–1731.
7. Ohtsuki, S., and Terasaki, T. (2007). Contribution of carrier-mediated transport systems to the blood-brain barrier as a supporting and protecting interface for the brain; importance for CNS drug discovery and development. Pharm. Res. *24*, 1745–1758.
8. Saitou, M., Furuse, M., Sasaki, H., Schulzke, J.D., Fromm, M., Takano, H., Noda, T., and Tsukita, S. (2000). Complex phenotype of mice lacking occludin, a component of tight junction strands. Mol. Biol. Cell *11*, 4131–4142.
9. von Tell, D., Armulik, A., and Betsholtz, C. (2006). Pericytes and vascular stability. Exp. Cell Res. *312*, 623–629.
10. Armulik, A., Abramsson, A., and Betsholtz, C. (2005). Endothelial/pericyte interactions. Circ. Res. *97*, 512–523.
11. Proescholdt, M.A., Heiss, J.D., Walbridge, S., Mühlhauser, J., Capogrossi, M.C., Oldfield, E.H., and Merrill, M.J. (1999). Vascular endothelial growth factor (VEGF) modulates vascular permeability and inflammation in rat brain. J. Neuropathol. Exp. Neurol. *58*, 613–627.
12. Argaw, A.T., Gurfein, B.T., Zhang, Y., Zameer, A., and John, G.R. (2009). VEGF-mediated disruption of endothelial CLN-5 promotes blood-brain barrier breakdown. Proc. Natl. Acad. Sci. USA *106*, 1977–1982.
13. Horng, S., Therattil, A., Moyon, S., Gordon, A., Kim, K., Argaw, A.T., Hara, Y., Mariani, J.N., Sawai, S., Flodby, P., et al. (2017). Astrocytic tight junctions control inflammatory CNS lesion pathogenesis. J. Clin. Invest. *127*, 3136–3151.
14. Sofroniew, M.V. (2015). Astrocyte barriers to neurotoxic inflammation. Nat. Rev. Neurosci. *16*, 249–263.
15. Haruwaka, K., Ikegami, A., Tachibana, Y., Ohno, N., Konishi, H., Hashimoto, A., Matsumoto, M., Kato, D., Ono, R., Kiyama, H., et al. (2019). Dual microglia effects on blood brain barrier permeability induced by systemic inflammation. Nat. Commun. *10*, 5816.
16. Bennett, M.L., Bennett, F.C., Liddelow, S.A., Ajami, B., Zamanian, J.L., Fernhoff, N.B., Mulinyawe, S.B., Bohlen, C.J., Adil, A., Tucker, A., et al. (2016). New tools for studying microglia in the mouse and human CNS. Proc. Natl. Acad. Sci. USA *113*, E1738–E1746.
17. Unger, M.S., Schernthaner, P., Marschallinger, J., Mrowetz, H., and Aigner, L. (2018). Microglia prevent peripheral immune cell invasion and promote an anti-inflammatory environment in the brain of APP-PS1 transgenic mice. J. Neuroinflammation *15*, 274.
18. Huber, J.D., Campos, C.R., Mark, K.S., and Davis, T.P. (2006). Alterations in blood-brain barrier ICAM-1 expression and brain microglial activation after lambda-carrageenan-induced inflammatory pain. Am. J. Physiol. Heart Circ. Physiol. *290*, H732–H740.
19. Pan, J., Ma, N., Yu, B., Zhang, W., and Wan, J. (2020). Transcriptomic profiling of microglia and astrocytes throughout aging. J. Neuroinflammation *17*, 97.
20. Perrino, B.A. (2016). Calcium Sensitization Mechanisms in Gastrointestinal Smooth Muscles. J. Neurogastroenterol. Motil. *22*, 213–225.

21. Eto, M., Senba, S., Morita, F., and Yazawa, M. (1997). Molecular cloning of a novel phosphorylation-dependent inhibitory protein of protein phosphatase-1 (CPI17) in smooth muscle: its specific localization in smooth muscle. FEBS Lett. *410*, 356–360.

22. Eto, M. (2009). Regulation of cellular protein phosphatase-1 (PP1) by phosphorylation of the CPI-17 family, C-kinase-activated PP1 inhibitors. J. Biol. Chem. *284*, 35273–35277.

23. Agarwal, V., Sroka, M., Fulde, M., Bergmann, S., Riesbeck, K., and Blom, A.M. (2014). Binding of Streptococcus pneumoniae endopeptidase O (PepO) to complement component C1q modulates the complement attack and promotes host cell adherence. J. Biol. Chem. *289*, 15833–15844.

24. Ermert, D., Weckel, A., Agarwal, V., Frick, I.-M., Björck, L., and Blom, A.M. (2013). Binding of complement inhibitor C4b-binding protein to a highly virulent Streptococcus pyogenes M1 strain is mediated by protein H and enhances adhesion to and invasion of endothelial cells. J. Biol. Chem. *288*, 32172–32183.

25. Griffith, A.A., and Holmes, W. (2019). Fine Tuning: Effects of Post-Translational Modification on Hsp70 Chaperones. Int. J. Mol. Sci. *20*, 4207.

26. Bobkova, N.V., Evgen'ev, M., Garbuz, D.G., Kulikov, A.M., Morozov, A., Samokhin, A., Velmeshev, D., Medvinskaya, N., Nesterova, I., Pollock, A., and Nudler, E. (2015). Exogenous Hsp70 delays senescence and improves cognitive function in aging mice. Proc. Natl. Acad. Sci. USA *112*, 16006–16011.

27. Fantin, A., Vieira, J.M., Gestri, G., Denti, L., Schwarz, Q., Prykhozhij, S., Peri, F., Wilson, S.W., and Ruhrberg, C. (2010). Tissue macrophages act as cellular chaperones for vascular anastomosis downstream of VEGF-mediated endothelial tip cell induction. Blood *116*, 829–840.

28. da Fonseca, A.C., Matias, D., Garcia, C., Amaral, R., Geraldo, L.H., Freitas, C., and Lima, F.R. (2014). The impact of microglial activation on blood-brain barrier in brain diseases. Front. Cell. Neurosci. *8*, 362.

29. Williams, K., Alvarez, X., and Lackner, A.A. (2001). Central nervous system perivascular cells are immunoregulatory cells that connect the CNS with the peripheral immune system. Glia *36*, 156–164.

30. Hawkins, B.T., and Davis, T.P. (2005). The blood-brain barrier/neurovascular unit in health and disease. Pharmacol. Rev. *57*, 173–185.

31. Neuwelt, E.A., Bauer, B., Fahlke, C., Fricker, G., Iadecola, C., Janigro, D., Leybaert, L., Molnár, Z., O'Donnell, M.E., Povlishock, J.T., et al. (2011). Engaging neuroscience to advance translational research in brain barrier biology. Nat. Rev. Neurosci. *12*, 169–182.

32. Daneman, R. (2012). The blood-brain barrier in health and disease. Ann. Neurol. *72*, 648–672.

33. Kelly, P., Denver, P., Satchell, S.C., Ackermann, M., Konerding, M.A., and Mitchell, C.A. (2017). Microvascular ultrastructural changes precede cognitive impairment in the murine APPswe/PS1dE9 model of Alzheimer's disease. Angiogenesis *20*, 567–580.

34. Montagne, A., Barnes, S.R., Sweeney, M.D., Halliday, M.R., Sagare, A.P., Zhao, Z., Toga, A.W., Jacobs, R.E., Liu, C.Y., Amezcua, L., et al. (2015). Blood-brain barrier breakdown in the aging human hippocampus. Neuron *85*, 296–302.

35. Sweeney, M.D., Sagare, A.P., and Zlokovic, B.V. (2018). Blood-brain barrier breakdown in Alzheimer disease and other neurodegenerative disorders. Nat. Rev. Neurol. *14*, 133–150.

36. Nation, D.A., Sweeney, M.D., Montagne, A., Sagare, A.P., D'Orazio, L.M., Pachicano, M., Sepehrband, F., Nelson, A.R., Buennagel, D.P., Harrington, M.G., et al. (2019). Blood-brain barrier breakdown is an early biomarker of human cognitive dysfunction. Nat. Med. *25*, 270–276.

37. van de Haar, H.J., Jansen, J.F.A., van Osch, M.J.P., van Buchem, M.A., Muller, M., Wong, S.M., Hofman, P.A.M., Burgmans, S., Verhey, F.R.J., and Backes, W.H. (2016). Neurovascular unit impairment in early Alzheimer's disease measured with magnetic resonance imaging. Neurobiol. Aging *45*, 190–196.

38. Stichel, C.C., and Luebbert, H. (2007). Inflammatory processes in the aging mouse brain: participation of dendritic cells and T-cells. Neurobiol. Aging *28*, 1507–1521.

39. Parameswaran, N., and Patial, S. (2010). Tumor necrosis factor-α signaling in macrophages. Crit. Rev. Eukaryot. Gene Expr. *20*, 87–103.

40. Lopez-Castejon, G., and Brough, D. (2011). Understanding the mechanism of IL-1β secretion. Cytokine Growth Factor Rev. *22*, 189–195.

41. Tugues, S., Burkhard, S.H., Ohs, I., Vrohlings, M., Nussbaum, K., Vom Berg, J., Kulig, P., and Becher, B. (2015). New insights into IL-12-mediated tumor suppression. Cell Death Differ. *22*, 237–246.

42. Fricker, L.D., McKinzie, A.A., Sun, J., Curran, E., Qian, Y., Yan, L., Patterson, S.D., Courchesne, P.L., Richards, B., Levin, N., et al. (2000). Identification and characterization of proSAAS, a granin-like neuroendocrine peptide precursor that inhibits prohormone processing. J. Neurosci. *20*, 639–648.

43. Jarvela, T.S., Lam, H.A., Helwig, M., Lorenzen, N., Otzen, D.E., McLean, P.J., Maidment, N.T., and Lindberg, I. (2016). The neural chaperone proSAAS blocks α-synuclein fibrillation and neurotoxicity. Proc. Natl. Acad. Sci. USA *113*, E4708–E4715.

44. Hoshino, A., Helwig, M., Rezaei, S., Berridge, C., Eriksen, J.L., and Lindberg, I. (2014). A novel function for proSAAS as an amyloid anti-aggregant in Alzheimer's disease. J. Neurochem. *128*, 419–430.

45. Helwig, M., Hoshino, A., Berridge, C., Lee, S.-N., Lorenzen, N., Otzen, D.E., Eriksen, J.L., and Lindberg, I. (2013). The neuroendocrine protein 7B2 suppresses the aggregation of neurodegenerative disease-related proteins. J. Biol. Chem. *288*, 1114–1124.

46. Kikuchi, K., Arawaka, S., Koyama, S., Kimura, H., Ren, C.-H., Wada, M., Kawanami, T., Kurita, K., Daimon, M., Kawakatsu, S., et al. (2003). An N-terminal fragment of ProSAAS (a granin-like neuroendocrine peptide precursor) is associated with tau inclusions in Pick's disease. Biochem. Biophys. Res. Commun. *308*, 646–654.

47. Wada, M., Ren, C.-H., Koyama, S., Arawaka, S., Kawakatsu, S., Kimura, H., Nagasawa, H., Kawanami, T., Kurita, K., Daimon, M., et al. (2004). A human granin-like neuroendocrine peptide precursor (proSAAS) immunoreactivity in tau inclusions of Alzheimer's disease and parkinsonism-dementia complex on Guam. Neurosci. Lett. *356*, 49–52.

48. Berezniuk, I., Rodriguiz, R.M., Zee, M.L., Marcus, D.J., Pintar, J., Morgan, D.J., Wetsel, W.C., and Fricker, L.D. (2017). ProSAAS-derived peptides are regulated by cocaine and are required for sensitization to the locomotor effects of cocaine. J. Neurochem. *143*, 268–281.

49. Ye, H., Wang, J., Tian, Z., Ma, F., Dowell, J., Bremer, Q., Lu, G., Baldo, B., and Li, L. (2017). Quantitative Mass Spectrometry Reveals Food Intake-Induced Neuropeptide Level Changes in Rat Brain: Functional Assessment of Selected Neuropeptides as Feeding Regulators. Mol. Cell. Proteomics *16*, 1922–1937.

50. Wardman, J.H., Berezniuk, I., Di, S., Tasker, J.G., and Fricker, L.D. (2011). ProSAAS-derived peptides are colocalized with neuropeptide Y and function as neuropeptides in the regulation of food intake. PLoS ONE *6*, e28152.

51. Finehout, E.J., Franck, Z., Choe, L.H., Relkin, N., and Lee, K.H. (2007). Cerebrospinal fluid proteomic biomarkers for Alzheimer's disease. Ann. Neurol. *61*, 120–129.

52. Abdi, F., Quinn, J.F., Jankovic, J., McIntosh, M., Leverenz, J.B., Peskind, E., Nixon, R., Nutt, J., Chung, K., Zabetian, C., et al. (2006). Detection of biomarkers with a multiplex quantitative proteomic platform in cerebrospinal fluid of patients with neurodegenerative disorders. J. Alzheimers Dis. *9*, 293–348.

53. Liu, M., Li, Y., Liu, Y., Yan, S., Liu, G., Zhang, Q., and Ji, B. (2019). Cold-inducible RNA-binding protein as a novel target to alleviate blood-brain barrier damage induced by cardiopulmonary bypass. J. Thorac. Cardiovasc. Surg. *157*, 986–996.e5.

54. Badhwar, A., Stanimirovic, D.B., Hamel, E., and Haqqani, A.S. (2014). The proteome of mouse cerebral arteries. J. Cereb. Blood Flow Metab. *34*, 1033–1046.

55. Kolosova, I.A., Ma, S.-F., Adyshev, D.M., Wang, P., Ohba, M., Natarajan, V., Garcia, J.G.N., and Verin, A.D. (2004). Role of CPI-17 in the regulation of endothelial cytoskeleton. Am. J. Physiol. Lung Cell. Mol. Physiol. *287*, L970–L980.

56. Wu, X., Fu, S., Liu, Y., Luo, H., Li, F., Wang, Y., Gao, M., Cheng, Y., and Xie, Z. (2019). NDP-MSH binding melanocortin-1 receptor ameliorates neuroinflammation and BBB disruption through CREB/Nr4a1/NF-κB pathway after intracerebral hemorrhage in mice. J. Neuroinflammation *16*, 192.

57. Popichak, K.A., Hammond, S.L., Moreno, J.A., Afzali, M.F., Backos, D.S., Slayden, R.D., Safe, S., and Tjalkens, R.B. (2018). Compensatory Expression of Nur77 and Nurr1 Regulates NF-κB-Dependent Inflammatory Signaling in Astrocytes. Mol. Pharmacol. *94*, 1174–1186.

58. You, B., Jiang, Y.Y., Chen, S., Yan, G., and Sun, J. (2009). The orphan nuclear receptor Nur77 suppresses endothelial cell activation through induction of IkappaBalpha expression. Circ. Res. *104*, 742–749.

59. Wang, F., Gao, Y., Tang, L., Ning, K., Geng, N., Zhang, H., Li, Y., Li, Y., Liu, F., and Li, F. (2019). A novel PAK4-CEBPB-CLDN4 axis involving in breast cancer cell migration and invasion. Biochem. Biophys. Res. Commun. *511*, 404–408.

60. Ruan, W., Li, J., Xu, Y., Wang, Y., Zhao, F., Yang, X., Jiang, H., Zhang, L., Saavedra, J.M., Shi, L., and Pang, T. (2019). MALAT1 Up-Regulator Polydatin Protects Brain Microvascular Integrity and Ameliorates Stroke Through C/EBPβ/MALAT1/CREB/PGC-1α/PPARγ Pathway. Cell. Mol. Neurobiol. *39*, 265–286.

61. El-Asmar, B., Giner, X.C., and Tremblay, J.J. (2009). Transcriptional cooperation between NF-kappaB p50 and CCAAT/enhancer binding protein beta regulates Nur77 transcription in Leydig cells. J. Mol. Endocrinol. *42*, 131–138.

62. Mildner, A., Schönheit, J., Giladi, A., David, E., Lara-Astiaso, D., Lorenzo-Vivas, E., Paul, F., Chappell-Maor, L., Priller, J., Leutz, A., et al. (2017). Genomic Characterization of Murine Monocytes Reveals C/EBPβ Transcription Factor Dependence of Ly6C$^-$ Cells. Immunity *46*, 849–862.e7.

63. Thuringer, D., and Garrido, C. (2019). Molecular chaperones in the brain endothelial barrier: neurotoxicity or neuroprotection? FASEB J. *33*, 11629–11639.

64. Rauch, J.N., and Gestwicki, J.E. (2014). Binding of human nucleotide exchange factors to heat shock protein 70 (Hsp70) generates functionally distinct complexes in vitro. J. Biol. Chem. *289*, 1402–1414.

65. Lau, S.-F., Cao, H., Fu, A.K.Y., and Ip, N.Y. (2020). Single-nucleus transcriptome analysis reveals dysregulation of angiogenic endothelial cells and neuroprotective glia in Alzheimer's disease. Proc. Natl. Acad. Sci. USA *117*, 25800–25809.

66. Fielder, A.H., Walport, M.J., Batchelor, J.R., Rynes, R.I., Black, C.M., Dodi, I.A., and Hughes, G.R. (1983). Family study of the major histocompatibility complex in patients with systemic lupus erythematosus: importance of null alleles of C4A and C4B in determining disease susceptibility. Br. Med. J. (Clin. Res. Ed.) *286*, 425–428.

67. Ceriello, A., Giugliano, D., Quatraro, A., Marchi, E., Barbanti, M., and Lefebvre, P. (1990). Possible role for increased C4b-binding-protein level in acquired protein S deficiency in type I diabetes. Diabetes *39*, 447–449.

68. Mostafa, G.A., and Shehab, A.A. (2010). The link of C4B null allele to autism and to a family history of autoimmunity in Egyptian autistic children. J. Neuroimmunol. *223*, 115–119.

69. Zorzetto, M., Datturi, F., Divizia, L., Pistono, C., Campo, I., De Silvestri, A., Cuccia, M., and Ricevuti, G. (2017). Complement C4A and C4B Gene Copy Number Study in Alzheimer's Disease Patients. Curr. Alzheimer Res. *14*, 303–308.

70. Paillasse, M.R., and de Medina, P. (2015). The NR4A nuclear receptors as potential targets for anti-aging interventions. Med. Hypotheses *84*, 135–140.

71. Chao, L.C., Wroblewski, K., Ilkayeva, O.R., Stevens, R.D., Bain, J., Meyer, G.A., Schenk, S., Martinez, L., Vergnes, L., Narkar, V.A., et al. (2012). Skeletal muscle Nur77 expression enhances oxidative metabolism and substrate utilization. J. Lipid Res. *53*, 2610–2619.

72. Rodríguez-Calvo, R., Tajes, M., and Vázquez-Carrera, M. (2017). The NR4A subfamily of nuclear receptors: potential new therapeutic targets for the treatment of inflammatory diseases. Expert Opin. Ther. Targets *21*, 291–304.

73. Tenga, A., Beard, J.A., Takwi, A., Wang, Y.-M., and Chen, T. (2016). Regulation of Nuclear Receptor Nur77 by miR-124. PLoS ONE *11*, e0148433.

74. Morin, C., Fortin, S., Cantin, A.M., and Rousseau, E. (2011). Docosahexaenoic acid derivative prevents inflammation and hyperreactivity in lung: implication of PKC-Potentiated inhibitory protein for heterotrimeric myosin light chain phosphatase of 17 kD in asthma. Am. J. Respir. Cell Mol. Biol. *45*, 366–375.

75. Ohama, T., Hori, M., Fujisawa, M., Kiyosue, M., Hashimoto, M., Ikenoue, Y., Jinno, Y., Miwa, H., Matsumoto, T., Murata, T., and Ozaki, H. (2008). Downregulation of CPI-17 contributes to dysfunctional motility in chronic intestinal inflammation model mice and ulcerative colitis patients. J. Gastroenterol. *43*, 858–865.

76. Li, J., Pang, J., Liu, Y., Zhang, J., Zhang, C., Shen, G., and Song, L. (2018). Suppression of RRM2 inhibits cell proliferation, causes cell cycle arrest and promotes the apoptosis of human neuroblastoma cells and in human neuroblastoma RRM2 is suppressed following chemotherapy. Oncol. Rep. *40*, 355–360.

77. Hu, S.F., Lin, X., Xu, L.P., Chen, H.G., Guo, J.F., and Jin, L. (2020). DCK is an Unfavorable Prognostic Biomarker and Correlated With Immune Infiltrates in Liver Cancer. Technol. Cancer Res. Treat. *19*, 1533033820934133.

78. Carvelli, J., Demaria, O., Vély, F., Batista, L., Chouaki Benmansour, N., Fares, J., Carpentier, S., Thibult, M.-L., Morel, A., Remark, R., et al.; Explore COVID-19 IPH group; Explore COVID-19 Marseille Immunopole group (2020). Association of COVID-19 inflammation with activation of the C5a-C5aR1 axis. Nature *588*, 146–150.

79. Hirase, T., Kawashima, S., Wong, E.Y., Ueyama, T., Rikitake, Y., Tsukita, S., Yokoyama, M., and Staddon, J.M. (2001). Regulation of tight junction permeability and occludin phosphorylation by Rhoa-p160ROCK-dependent and -independent mechanisms. J. Biol. Chem. *276*, 10423–10431.

80. Nusrat, A., Giry, M., Turner, J.R., Colgan, S.P., Parkos, C.A., Carnes, D., Lemichez, E., Boquet, P., and Madara, J.L. (1995). Rho protein regulates tight junctions and perijunctional actin organization in polarized epithelia. Proc. Natl. Acad. Sci. USA *92*, 10629–10633.

81. Persidsky, Y., Heilman, D., Haorah, J., Zelivyanskaya, M., Persidsky, R., Weber, G.A., Shimokawa, H., Kaibuchi, K., and Ikezu, T. (2006). Rho-mediated regulation of tight junctions during monocyte migration across the blood-brain barrier in HIV-1 encephalitis (HIVE). Blood *107*, 4770–4780.

82. Kim, E.K., and Choi, E.J. (2010). Pathological roles of MAPK signaling pathways in human diseases. Biochim. Biophys. Acta *1802*, 396–405.

83. Wang, Y., Zhang, J., Yi, X.J., and Yu, F.S. (2004). Activation of ERK1/2 MAP kinase pathway induces tight junction disruption in human corneal epithelial cells. Exp. Eye Res. *78*, 125–136.

84. Chen, Yh., Lu, Q., Schneeberger, E.E., and Goodenough, D.A. (2000). Restoration of tight junction structure and barrier function by down-regulation of the mitogen-activated protein kinase pathway in ras-transformed Madin-Darby canine kidney cells. Mol. Biol. Cell *11*, 849–862.

85. Dörfel, M.J., and Huber, O. (2012). Modulation of tight junction structure and function by kinases and phosphatases targeting occludin. J. Biomed. Biotechnol. *2012*, 807356.